

1 **Anaerobic nitrogen cycling on a Neoproterozoic ocean margin**

2 **Mettam, C.^{a,b*}, Zerkle, A.L.^a, Claire, M.W.^a, Prave, A.R.^a, Poulton, S.W.^c, Junium, C.K.^d**

3

4 ^a **School of Earth & Environmental Sciences, University of St Andrews, Irvine Building, St Andrews,**
5 **Fife, KY16 9AL, United Kingdom.**

6 ^b **Department of Earth Sciences, University College London, 5 Gower Place, London, WC1E 6BS,**
7 **United Kingdom (current address).**

8 ^c **School of Earth and Environment, University of Leeds, Leeds LS2 9JT, United Kingdom.**

9 ^d **Department of Earth Science, Syracuse University, NY 13244-1070, USA.**

10 *** Corresponding author**

11

12 **Abstract**

13 A persistently aerobic marine nitrogen cycle featuring the biologically mediated oxidation of
14 ammonium to nitrate has likely been in place since the Great Oxidation Event (GOE) some 2.3 billion
15 years ago. Although nitrogen isotope data from some Neoproterozoic sediments suggests transient
16 nitrate availability prior to the GOE, these data are open to other interpretations. This is especially so
17 as these data come from deep-water environments that were spatially divorced from shallow-water
18 settings that were the most likely sites for the accumulation of oxygen and the generation of nitrate.
19 Here we present the first nitrogen isotope data from contemporaneous shallow-water sediments to
20 constrain the nitrogen cycle in shallow Late Archean settings. The BH-1 Sacha core through the
21 Campbellrand-Malmani carbonate platform records a transition from a shallow
22 siliciclastic/carbonate ramp to a rimmed carbonate shelf with the potential for reduced
23 communication with the open ocean. In these settings nitrogen isotope ($\delta^{15}\text{N}$) data from sub- to

24 peri-tidal and lagoonal settings are close to 0‰, indicating diazotrophy or the complete utilization of
25 remineralised ammonium with an isotopic composition of near 0‰. Our dataset also includes
26 negative $\delta^{15}\text{N}$ values that suggest the presence of an ammonium pool of concentrations sufficient to
27 have allowed for non-quantitative assimilation. We suggest that this condition may have been the
28 result of upwelling of phosphorus-rich deep waters into the photic zone, stimulating primary
29 productivity and creating an enhanced flux of organic matter that was subsequently remineralised
30 and persisted in the dominantly anoxic Neoproterozoic marine environment. Notably, we find only
31 limited evidence of coupled nitrification/denitrification, even in these shallow water environments,
32 calling into question previous suggestions that the Late Archean nitrogen cycle was characterized by
33 widespread aerobic nitrogen cycling. Rather, aerobic nitrogen cycling was likely spatially
34 heterogeneous and tied to loci of high oxygen production while zones of shallow water anoxia
35 persisted.

36

37 Keywords

- 38 • Nitrogen Isotopes
- 39 • Carbon Isotopes
- 40 • Neoproterozoic

41

42

43

44

45

46

47 **1. Introduction**

48 Nitrogen (N) is an essential nutrient for the construction of all biomolecules. Despite the biological
49 importance of N_2 and its abundance in the atmosphere, only diazotrophic (N_2 -fixing) microbes can
50 directly assimilate di-nitrogen into biomass, which ultimately provides the primary source of
51 nitrogen to the biosphere. In the absence of oxygen, the uptake of ammonium (NH_4^+) from
52 remineralised diazotrophic biomass is the primary source of nitrogen for non-diazotrophs. In oxygen-
53 rich waters, NH_4^+ is rapidly recycled or oxidised by nitrifying microbes to nitrite (NO_2^-) and nitrate
54 (NO_3^-). Nitrate is an important component of dissolved inorganic nitrogen (DIN) in oxygenated
55 waters, and serves as the dominant nitrogen source for primary productivity in modern surface
56 oceans. In such conditions diazotrophic activity will be reduced due to competition with nitrate
57 assimilators for other nutrients (e.g. Sigman et al., 2009).

58 In low-oxygen settings, such as modern oxygen minimum zones (OMZs), NO_2^- and NO_3^- can also be
59 utilised as electron acceptors in chemotrophic metabolisms. For example, NO_3^- can be used in
60 heterotrophic denitrification or during dissimilatory nitrate reduction to ammonium (DNRA)
61 (Granger et al., 2008), whilst NO_2^- is utilised in the anaerobic oxidation of ammonium (anammox).
62 Importantly, both anammox and denitrification remove bioavailable nitrogen from the oceanic
63 reservoir and return it to the atmosphere (Cline and Kaplan, 1975), which in extreme cases can lead
64 to nitrate limitation. When bioavailable nitrogen is scarce an expansion of diazotrophy can occur due
65 to reduced competition for nutrients, if other nutrients like Fe or bioactive trace elements are not
66 limiting (Weber and Deutsch, 2013; Sigman et al., 2009).

67 Due to the redox sensitive nature of these N cycling processes, the global N cycle is believed to have
68 evolved over geologic time alongside changes in the redox state of Earth's oceans and atmosphere
69 (e.g., Stüeken et al., 2016). The 2.33 Ga Great Oxidation Event (GOE) (Luo et al., 2016) marked the
70 time when atmospheric oxygen (O_2) first exceeded 10^{-5} times present atmospheric levels (PAL), as
71 constrained by the disappearance of mass-independent fractionation (MIF) of sulphur isotopes

72 (Farquhar et al., 2011; Pavlov and Kasting, 2002). This change in surface redox conditions seemingly
73 coincided with the widespread expansion of aerobic nitrogen cycling in the world's oceans (e.g.,
74 Zerkle et al., 2017; Luo et al., 2018). However, this narrative could be overly simplistic. In particular,
75 small increases of around 2‰ in $\delta^{15}\text{N}$ values are preserved in the 2.7-2.5 Ga sediments of the
76 Campbellrand-Malmani carbonate platform from South Africa (Godfrey and Falkowski, 2009), a
77 setting that is spatially and temporally correlated to the sediments analysed in this study, albeit
78 further offshore and a deeper depositional setting. Other positive excursions in $\delta^{15}\text{N}$ are reported
79 from studies of Australian Neoproterozoic sediments (Garvin et al., 2009; Busigny et al., 2013) and in
80 all settings these nitrogen isotope values have been explained by transient or localized aerobic
81 nitrogen cycling. Alternatively, these small positive shifts in $\delta^{15}\text{N}$ values could represent uptake of a
82 residual pool of ^{15}N -enriched ammonium produced by partial nitrification or partial assimilation, or
83 by nitrogen redox cycling independent of environmental oxygenation (e.g., Thomazo et al., 2011;
84 Busigny et al., 2013; Ader et al., 2016). However, there are currently no $\delta^{15}\text{N}$ records of
85 contemporaneous shallow-water sediments available to distinguish between these alternatives.

86 Here, we investigate $\delta^{15}\text{N}$ values preserved in shallow-water sediments from the 2.7-2.5 Ga
87 Campbellrand-Malmani carbonate platform. These sediments, from the BH-1 Sacha core, represent
88 the shallow-water equivalent to previously investigated deeper-water sediments (GKP01 core;
89 Fischer et al., 2009), in which $\delta^{15}\text{N}$ values rose by about 2‰ and were interpreted to represent
90 transient aerobic nitrogen cycling (Godfrey and Falkowski, 2009). If aerobic nitrogen cycling was
91 even intermittently pervasive in this basin, we would expect sediments from these shallower water
92 settings to record similar $\delta^{15}\text{N}$ values to deeper-water sediments, particularly given their potential
93 proximity to surface ocean oxygen oases, as shown by the presence of microbial sedimentary
94 structures (Altermann and Siegfried, 1997).

95

96

97 2. Tracking the nitrogen cycle through time

98 Transformations in the marine nitrogen cycle can modify nitrogen isotope signals ($^{15}\text{N}/^{14}\text{N}$; $\delta^{15}\text{N}$ (‰)
99 = $((^{15}\text{N}/^{14}\text{N})_{\text{sample}} / (^{15}\text{N}/^{14}\text{N})_{\text{air}} - 1) \times 1000$), leading to fractionation effects between the reactants and
100 products (Casciotti, 2009; Sigman et al., 2009; Zerkle et al., 2008; Brunner et al., 2013; Möbius, 2013;
101 Zhang et al., 2014; McCready et al., 1983; Ader et al., 2016). However, in modern settings, most
102 nitrogen assimilation or redox transformations utilise all available substrates, leading to no apparent
103 fractionation effects (Sigman et al., 2009). The exceptions are diazotrophy and nitrate/nitrite-
104 reduction processes, including denitrification, DNRA, and anammox. Diazotrophy generally produces
105 biomass with $\delta^{15}\text{N}$ values between $\sim+1$ and $\sim-1\%$ (Zhang et al., 2014; Bauersachs et al., 2009),
106 although extreme values as low as $\sim-4\%$ have been experimentally demonstrated (e.g., as reviewed
107 in Zerkle et al., 2008). The contribution of diazotrophy to total biomass in modern ocean settings is
108 limited except under oligotrophic conditions, as NO_3^- and NH_4^+ assimilators compete more
109 successfully for other nutrients (Weber and Deutsch, 2013). However, in most oxygen-rich settings,
110 NH_4^+ sourced from remineralised biomass is rapidly oxidized, such that nitrate is the main form of
111 nutrient N. In the modern ocean incomplete denitrification in the water column renders this pool of
112 bioavailable ^{15}N -enriched, leading to marine organic matter (OM) with an average $\delta^{15}\text{N}$ of $+5$ ‰ to
113 $+6\%$ (Peters et al., 1978; Sigman et al., 2003; Galbraith et al., 2013).

114 The $\delta^{15}\text{N}$ of marine biomass thus records the dominant forms of bioavailable nitrogen utilised for
115 primary productivity, particularly on a local scale. These signals are ultimately archived in
116 sedimentary rocks, either directly in OM or retained as mineral-associated nitrogen derived from
117 degraded OM (e.g., Stüeken et al., 2016; Freudenthal et al., 1999). Variations in the $\delta^{15}\text{N}$ of
118 sedimentary rocks can thus be utilized to track changes in the marine nitrogen cycle through
119 geological time.

120 3. Geological setting

121 The Campbellrand-Malmani Platform in South Africa (Fig. 1A, B and C) is part of the Transvaal
122 Supergroup. A ~3,700 m section of these rocks was recovered in the BH1-Sacha core and logged in
123 detail by Altermann and Siegfried (1997). The lowermost recovered strata are a succession of
124 interbedded doloarenites, quartzites, and shales with microbial laminites from the top of the
125 Vryburg Formation (Fm) (Altermann and Siegfried, 1997). Thick (> 10 m) shale beds in the lower part
126 of the core likely represent deeper shelf conditions when marine transgressions mark the beginning
127 of several deepening and shallowing cycles, with carbonates likely representative of the shallowest
128 regressive conditions. Thin (< 10 m) shales interbedded with carbonates throughout the core are
129 mostly likely evidence of slightly deeper lagoonal conditions during generally regressive periods
130 (Altermann and Siegfried, 1997). A major flooding surface defines the base of the overlying
131 Boomplaas Fm, but its top is defined by an oolite bed indicating shallow, wave-agitated conditions.
132 The Lokammona Fm is marked by several, variably developed, shoaling cycles similar to those in the
133 Vryburg Fm (Sumner and Beukes, 2006). These three formations comprise the Schmidtsdrift
134 Subgroup, and are overlain by the Monteville Fm of the lowermost Campbellrand Subgroup, which
135 shows cycles similar to the Lokammona Fm (Sumner and Beukes, 2006). Together, these four
136 formations are interpreted as representing deposition of sediments on an evolving ramp structure
137 (Fig. 1B).

138 From the Reivilo Fm upwards, depositional conditions are considered to have been generally
139 shallow, with subtidal, intertidal or lagoonal conditions dominating as inferred from the presence of
140 domal, columnar, elongate and small, bifurcating, finger-like stromatolites, birds-eye structures, flat-
141 pebble breccias and chert beds (Altermann and Siegfried, 1997; Sumner and Beukes, 2006; Fischer
142 and Knoll, 2009). These facies are considered to represent the replacement of ramp-like conditions
143 with a rimmed-, carbonate-dominated shallow-shelf, platform-top (Sumner and Grotzinger, 2004;
144 Sumner and Beukes 2006). A maximum metamorphic grade of sub-greenschist is reported for the
145 section of the Campbellrand-Malmani Platform studied here (Button, 1973; Miyano and Beukes,
146 1984; Fischer et al., 2009), consistent with minimal alteration of stable isotope values as indicated by

147 our data (see discussion below). A U-Pb zircon age of $2,714 \pm 8$ Ma from the underlying Ventersdorp
148 Supergroup provides a maximum age for the Campbellrand-Malmani Platform (Armstrong et al.,
149 1991) and tuffs within the Schmidtsdrift and Campbellrand subgroups have yielded stratigraphically
150 coherent Neoarchaeon ages (Barton et al., 1995; Walraven and Martini, 1995; Fischer et al., 2009;
151 Knoll and Beukes, 2009; ranges of published dates are in the supplementary material).

152 **4. Methods**

153 Samples were collected from the National Core Repository at Donkerhoek (Pretoria, South Africa).
154 Sampling was predominantly focussed on black shales, which were anticipated to have high-TOC
155 content. Samples were ground into homogenous powders in agate ball mills, and carbonate was
156 removed via two 24 hour digestions in 10 % (vol/vol) HCl. After each digestion the samples were
157 centrifuged and the supernatant was discarded and replaced with fresh 10% HCl. Sample residues
158 were washed until pH neutral using ultrapure water ($18.2 \text{ M}\Omega\cdot\text{cm}$) and dried at < 40 °C. Carbonate
159 content was calculated gravimetrically from dry sample residues which were then homogenised
160 using an agate pestle and mortar and stored in glass vials. Several samples of mid-grey carbonate
161 rocks, assumed to contain some OM, were also decarbonated to assess the possibility of extracting
162 kerogen. This method of carbonate abundance determination is prone to inaccuracy. However, here
163 it is used only to provide a broad assessment of lithological characteristics, for example between
164 rocks with high carbonate content (e.g. $> 85\%$), and those with low carbonate concentrations (e.g.
165 $< 10\%$). Kerogen was extracted at the University of St Andrews by digestion of decarbonated residues
166 in HF/HCl following established protocols (e.g., Zerkle et al., 2017).

167 Nitrogen isotope values for kerogen ($\delta^{15}\text{N}_{\text{org}}$) and decarbonated sediments ($\delta^{15}\text{N}_{\text{bulk}}$) were
168 determined by nano-EA-IRMS in the GAPP Lab at Syracuse University, USA. Prior to analyses,
169 samples and standards were placed into a vacuum chamber overnight to remove atmospheric
170 nitrogen and flooded with Argon (Ar) prior to analysis. Upon introduction into the EA, tin capsule
171 sealed samples were further purged with helium (He) for 45 seconds prior to combustion in an

172 Elemental Vario Isotope Cube coupled to a Trace Gas analyser. Oxidation and reduction reactor
173 temperatures were 1100 °C and 650 °C, respectively. Helium carrier gas flow was 150 ml/min; and
174 the O₂ pulse was set for 90 seconds. Resultant sample gas was trapped in a liquid-N silica gel filled
175 cryotrap, before release to an Elemental Isoprime 100 IRMS via an Agilent CarboBond capillary
176 column (25 m x 0.53 mm x 5 um) with a He flow rate of ~2 cm³ min⁻¹ (e.g., Polissar et al., 2008; Zerkle
177 et al., 2017; Luo et al., 2018).

178 Data accuracy for δ¹⁵N_{org} was assessed using the IAEA N1 (Ammonium Sulphate, (NH₄)₂ SO₄) standard
179 which provided a mean δ¹⁵N value of 0.11 ± 0.50‰ (1σ; n=30) versus a certified value of +0.40 ±
180 0.2‰ (1σ).

181 The extremely sensitive nature of the nano-EA-IRMS method generates relatively large peak height
182 sizes for the blank, in comparison to standard IRMS techniques. This, coupled with relatively
183 nitrogen-poor kerogen samples, led to blank-sample ratios that could introduce variability in δ¹⁵N_{org}
184 measurements. Blank-corrected δ¹⁵N_{org} were calculated by blank extraction using the following
185 equation:

$$186 \quad \delta^{15}\text{N}_{\text{org}} = \frac{(\text{Peak Area}_{\text{sample}} * \delta^{15}\text{N}_{\text{sample}}) - (\text{Peak Area}_{\text{blank}} * \delta^{15}\text{N}_{\text{blank}})}{(\text{Peak Area}_{\text{sample}} - \text{Peak Area}_{\text{blank}})}$$

187 The size (Peak Area_{blank}) and isotopic composition of the blank (δ¹⁵N_{blank}) contribution to each
188 sample measurement was calculated by measuring a blank (without tin cup - as we have found no
189 difference in blank size and isotopic value whether a tin cup was included or not) before and after
190 each five samples and calculating incremental change for both values between the two blanks.

191 Duplicates of sample BH1-330, corrected to IAEA N1 indicate reproducibility of δ¹⁵N_{org} was ± 0.02‰
192 (1σ), whilst triplicates of samples BH1-1963 and BH1-3144.33 produced values ± 0.49‰ (1σ) and ±
193 0.32‰ (1σ), respectively. Duplicates of samples with large blank contributions resulting from
194 exceptionally low N_{org} produced higher variability, resulting in δ¹⁵N_{org} measurements on samples
195 below 0.05 wt. % N being discarded. Error bars for δ¹⁵N_{org} plots were calculated using standard

196 deviation of triplicates (BH1-1963.6; 0.49‰) and standard deviation of standards (0.50‰; n=30),
197 where error bar = $\sqrt{(\text{error of standards}^2 + \text{largest error of corrected sample}^2)}$.

198 Decarbonated sediments were also analysed to measure $\delta^{15}\text{N}_{\text{bulk}}$ values. Again, nitrogen abundances
199 in these decarbonated residues (TN_{bulk}) were exceptionally low, ranging from 0.0018 wt. % to 0.017
200 wt. %, so samples were run in triplicate and $\delta^{15}\text{N}_{\text{bulk}}$ values determined by Keeling plots. These
201 samples were corrected to the reference material NIST1547 – Peach Leaves, which returned a $\delta^{15}\text{N}$
202 value of +1.76‰ (n=8, determined by Keeling plots) against a certified value of +1.98‰ for
203 measurement of triplicate samples and +2.10‰ (n=5) for sample 3364 reruns (Table S4). Error bars
204 for $\delta^{15}\text{N}_{\text{bulk}}$ reflect the combined standard deviation of standards and the intercept errors of keeling
205 plots for each individual sample triplicate using the same formula. These individual errors are shown
206 in supplementary table four.

207 Organic carbon isotope values ($\delta^{13}\text{C}_{\text{org}}$) for this study were measured at the University of St Andrews
208 via flash-combustion of decarbonated residues using a Costech 4010 EA equipped with a zero blank
209 autosampler and interfaced with a Thermo Finnigan Delta Plus XP IRMS in continuous flow mode.
210 Data accuracy was verified using an internal standard (n=5), and returned values of $-25.07 \pm 0.18\%$
211 (1σ) and $-25.05 \pm 0.11\%$ (1σ) against an accepted value of -25.04% .

212 Nitrogen and carbon isotope values are reported using the standard delta notation showing per mil
213 deviations from V-PDB for $\delta^{13}\text{C}$, and relative to N_{air} for $\delta^{15}\text{N}$.

214 The abundance of nitrogen in kerogen (N_{org}) and in decarbonated residues (TN_{bulk}) and the total
215 organic carbon content (TOC) of whole rock powders were calculated by comparing peak areas
216 generated during isotope analyses with those of standards with known abundances (Table S3 and
217 S4). To calculate TOC abundances, the carbon yield was adjusted according to the mass lost during
218 decarbonation.

219 Potassium (K) and iron (Fe) abundances for samples 2709 and 3364 were determined by XRF at
220 Department of Earth and Environment, Franklin and Marshall College, USA. Standards returned 0.51
221 wt. % ± 0.0014 (1σ) against a certified value of 0.52 wt. % for K_2O and 12.42 wt. % ± 0.0135 (1σ)
222 against a certified value of 12.30 wt. % for Fe_2O_3 . Data for the remaining four samples were analysed
223 at University of St Andrews using standard XRF providing a standard deviation of 1σ of 0.02 wt. % for
224 K_2O .

225 5. Results

226 Nitrogen isotope values from kerogen ($\delta^{15}N_{org}$) for BH1-Sacha (Fig. 2; Table 1) range from -2.73‰ to
227 $+3.18\text{‰}$ (mean $-0.23 \pm 1.59\text{‰}$ here and elsewhere, 1σ , $n=21$). With the exception of samples BH1-
228 3113.32 and BH1- 3144.33, all $\delta^{15}N_{org}$ values of greater than 0‰ are from samples with carbonate
229 abundance in excess of 85% (Fig. 2; Table S1). Bulk nitrogen isotope values ($\delta^{15}N_{bulk}$) range from $-$
230 3.30‰ to $+2.94\text{‰}$ (mean $+0.58 \pm 2.14\text{‰}$, $n=6$). Organic carbon isotope values ($\delta^{13}C_{org}$) for BH1-Sacha
231 (Fig. 2; Table S1, including a subset from Izon et al. [2015]) range from -46.09‰ to -27.36‰ (mean
232 $-36.69 \pm 3.76\text{‰}$, $n=26$).

233 For data binned by depositional setting, the ramp-top settings of the Schmidtsdrift Subgroup and
234 overlying Monteville Fm have mean $\delta^{15}N_{bulk}$ values of $+0.11 \pm 2.01\text{‰}$ ($n=5$) and $\delta^{15}N_{org}$ values of
235 $+0.22 \pm 1.96\text{‰}$, $n=7$ (Fig. 2; Table S1). The highest $\delta^{15}N_{org}$ values measured are from two carbonate-
236 rich facies: $+2.48\text{‰}$ at 3306.3 m core depth, and $+3.18\text{‰}$ at 3114.5 m. The highest and lowest $\delta^{15}N_{org}$
237 values from siliciclastic facies in this section are $+0.53\text{‰}$ and -2.03‰ , whilst $\delta^{15}N_{bulk}$ values range
238 from -3.30‰ to $+2.02\text{‰}$. Mean $\delta^{13}C_{org}$ values from these ramp depositional settings are $-34.27 \pm$
239 3.63‰ , $n=11$.

240 In the platform- top/ rimmed-shelf facies from the base of the Reivilo Fm through the Gamohaam
241 Fm, the mean $\delta^{15}N_{org}$ values are $-0.52 \pm 1.36\text{‰}$ ($n=15$) with a single $\delta^{15}N_{bulk}$ value of $+2.94\text{‰}$ (Fig. 2;
242 Table S1). Again, the three carbonate samples had significantly higher $\delta^{15}N$ values, up to $+3.17\text{‰}$.
243 Mean $\delta^{13}C_{org}$ values for these facies are $-38.13 \pm 3.26\text{‰}$ ($n=15$).

244 6. Discussion

245 6.1. Preservation of Primary Isotopic Signals

246 Diagenetic and metamorphic processes can produce changes in primary carbon and nitrogen isotope
247 values, generally driving $\delta^{13}\text{C}_{\text{org}}$ and $\delta^{15}\text{N}$ values heavier and/or causing a divergence between bulk
248 rock and kerogen $\delta^{15}\text{N}$. At the sub-greenschist facies conditions of the Campbellrand-Malmani
249 Platform (Button, 1973; Miyano and Beukes, 1984; Fischer et al., 2009) such effects should be
250 minimal, and not exceed 1 – 2‰ (Stüeken et al., 2017). However, we examined trends in stable
251 isotope values alongside elemental abundances to evaluate possible contributions from post-
252 depositional alteration.

253 Thermal maturation during diagenetic or metamorphic processes can preferentially remove ^{12}C and
254 ^{14}N from sediments, leading to diagnostic positive correlations between $\delta^{15}\text{N}_{\text{bulk}}$ and $\delta^{13}\text{C}_{\text{org}}$, and
255 negative correlations between the abundances of TOC and $\delta^{13}\text{C}_{\text{org}}$, the abundances of TN_{org} and
256 $\delta^{15}\text{N}_{\text{org}}$, and the abundances of TN_{bulk} and $\delta^{15}\text{N}_{\text{bulk}}$. We note a weak positive correlation between TN_{org}
257 and $\delta^{15}\text{N}_{\text{org}}$ ($R^2 = 0.28$; Fig. 3A) and a moderately positive correlation between TN_{bulk} and $\delta^{15}\text{N}_{\text{bulk}}$ ($R^2 =$
258 0.51 ; Fig. 3E). We also note a weak positive correlation between $\delta^{15}\text{N}_{\text{org}}$ and $\delta^{13}\text{C}_{\text{org}}$ ($R^2 = 0.24$; Fig.
259 3B) and a weak negative correlation between $\text{TOC}/\text{TN}_{\text{org}}$ and $\delta^{15}\text{N}_{\text{org}}$ ($R^2 = 0.37$, Fig. 3C). We note no
260 correlation between TOC and $\delta^{13}\text{C}_{\text{org}}$ ($R^2 = 0.10$; Fig. 3D), and no correlation between $\delta^{15}\text{N}_{\text{bulk}}$ and
261 $\delta^{13}\text{C}_{\text{org}}$ ($R^2 = 0.05$; Fig. 3F). Therefore, our data show little evidence for significant post-depositional
262 alteration of $\delta^{13}\text{C}_{\text{org}}$ or $\delta^{15}\text{N}$, consistent with the low metamorphic grade of these sediments. We also
263 examine the potential influence of nitrogen adsorbed onto detrital clays by comparing potassium (K)
264 content with TN_{bulk} and $\delta^{15}\text{N}_{\text{bulk}}$ (Figs. 3G and H).

265 We do note that there is a moderate correlation ($R^2 = 0.69$) between K and $\delta^{15}\text{N}_{\text{bulk}}$ suggesting that
266 higher concentrations of clay-bound ammonium could be associated with more-positive $\delta^{15}\text{N}_{\text{bulk}}$
267 values, although, this correlation is somewhat influenced by the one sample in this small data set.

268 The sample from 3364m is unusual in that negative (-3.3‰) $\delta^{15}\text{N}_{\text{bulk}}$ values are associated with very
269 low K abundances (0.97%) in comparison to the remaining samples (Table S6). When this sample is
270 removed from the analyses the correlation between K and $\delta^{15}\text{N}_{\text{bulk}}$ is more modest ($R^2 = 0.32$) which
271 more closely reflects the very limited correlation ($R^2 = 0.17$) between TN_{bulk} and K abundances.

272

273 **6.2. Nitrogen cycling in a marginal marine environment**

274 The majority of samples analysed in this study are from relatively thin shale units that were
275 intercalated with stromatolitic carbonates. These thin shales are interpreted to have been deposited
276 during small marine transgressions, overprinted upon longer-term, relatively shallow, potentially
277 lagoonal conditions in platform and ramp-top settings (Altermann and Siegfried, 1997; Sumner and
278 Beukes, 2006; Ergolu et al., 2017). These thin shales are distinct from thicker shale units that likely
279 represent more open and deeper marine settings. Given the shallow nature of this setting and the
280 presence of microbial mats within the photic zone, such conditions should be prime candidates for
281 pre-GOE oxygen oases. Although the persistence of sulphur MIF in the BH-1 Sacha record indicates
282 that atmospheric oxygen concentrations must have remained less than 1 ppm during this time (Izon
283 et al., 2015), oxygen concentrations could have been sufficiently high in the water column or locally
284 associated with benthic microbial mats to allow for aerobic biogeochemical cycling. Indeed, trace
285 element and iron speciation analyses from Neoproterozoic sediments of the Campbellrand-Malmani
286 Platform suggest a stratified ocean with mildly oxygenated surface oxygen oases (Kendall et al.,
287 2010; Czaja et al., 2012; Eroglu et al., 2015) and localized oxygen production in microbial mats
288 (Zerkle et al., 2012). Previous studies of trends in $\delta^{15}\text{N}$ from deeper water sediments from this basin
289 have also been interpreted to represent transient aerobic N cycling (Godfrey and Falkowski, 2009).

290 We find that $\delta^{15}\text{N}_{\text{org}}$ values from siliciclastic sediments deposited in these near-shore settings are
291 inconsistent with widespread coupled nitrification /denitrification. In particular, $\delta^{15}\text{N}$ values close to

292 0‰ are more consistent with a nitrogen cycle dominated by diazotrophy and the recycling of NH_4^+ ,
293 and suggest that any NO_3^- generated from localized oxidation of ammonium was quantitatively and
294 rapidly removed by denitrification and anammox. Even if NO_3^- was present, it likely provided a
295 secondary nutrient N source given that ammonium could have been persistently available under
296 widely anoxic water column conditions. In modern settings (e.g., Higgins et al., 2012) cyanobacteria
297 can assimilate both NH_4^+ and NO_3^- as a source of nitrogen, and it has been noted that genes
298 controlling the assimilation of oxidised nitrogen sources can be repressed in the presence of
299 ammonium (Flores et al., 2005).

300 The lower part of the BH1-Sacha core (e.g., the Schmidtdrift Subgroup and Monteville Fm)
301 represents depositional conditions that were likely open to the ocean. Both $\delta^{15}\text{N}_{\text{bulk}}$ and $\delta^{15}\text{N}_{\text{org}}$
302 values in these ramp facies (with the exception of samples at 3114.5m and 3306.3m, discussed
303 below) are again consistent with anaerobic nitrogen cycling. Intriguingly, one sample (3364m)
304 provided a $\delta^{15}\text{N}_{\text{bulk}}$ value of -3.3‰ , and another sample (3125.05m) a $\delta^{15}\text{N}_{\text{org}}$ value of -2.0‰ ,
305 showing greater ^{15}N depletion than biomass generally produced by modern marine diazotrophs. This
306 is especially the case when considering that the long-term diagenetic or metamorphic effects could
307 possibly have elevated $\delta^{15}\text{N}$ by a few per mille in comparison to the $\delta^{15}\text{N}$ of primary organic matter.
308 We suggest that these strongly negative $\delta^{15}\text{N}$ values indicate the generation of biomass from partial
309 assimilation of NH_4^+ , as recently suggested for ~ 2.7 Ga sediments (Yang et al., 2019). Ammonium
310 could have accumulated in deep waters under upwelling zones that supported high rates of
311 diazotrophic productivity and organic matter export (Fig. 4A, B). The remineralisation of this organic
312 matter at depth under anoxic conditions could have led to the formation of a deep-water NH_4^+ pool.
313 In turn, these ammonium-rich waters could have been upwelled, leading to partial NH_4^+ assimilation
314 by primary producers, thus forming ^{15}N -depleted organic matter. Such settings could have included
315 the ramp front during early platform formation (e.g., thicker shale units at 3364m) and later the
316 mature platform front (the latter a depositional setting not recorded in the BH1-Sacha core), both of
317 which represented relatively deeper conditions in contrast to shallow lagoonal depositional settings.

318 Other negative $\delta^{15}\text{N}$ values (e.g., those associated with thin shales intercalated with carbonates)
319 could represent times when communication between the lagoonal setting and the open ocean was
320 more vigorous and allowed NH_4^+ -rich deep waters to temporarily inundate the lagoon.

321 Sediments at 3364m have high Fe concentrations (14.8%; Table S6) that approach the lower
322 boundary of Fe abundances in banded iron formations, despite being deposited in open-ramp
323 conditions. It is possible that in these Fe-rich conditions, diazotrophs utilizing the FeMo nitrogenase
324 enzyme produced biomass with $\delta^{15}\text{N}$ values down to -4‰, similar to those reported in Zerkle et al.
325 (2008). In addition, diazotrophs using alternative nitrogenase enzymes (e.g., Fe-Fe or Fe-V) have
326 been shown to produced biomass with $\delta^{15}\text{N}$ values down to -7‰ when Mo is limited (Zhang et al.,
327 2014). However, large variations in $\delta^{98}\text{Mo}$ have been reported for the lower Campbellrand-Malmani
328 Platform, which provide evidence for a sizeable Mo reservoir (Eroglu et al., 2015). It is therefore
329 unlikely that diazotrophs would have relied on these less efficient alternative enzymes in this
330 environment.

331 Such low $\delta^{15}\text{N}$ values are unusual, but not unreported in modern oceans and in the more recent
332 geologic past (e.g. Higgins et al., 2012). For example, $\delta^{15}\text{N}$ values of $\sim -5\text{‰}$ have been reported for
333 particulate nitrogen, and attributed to the partial utilization of ammonium (Rau et al., 1991) and
334 nitrate (Altabet and Francois, 1994). In the latter case, these low values are associated with
335 incomplete utilisation of nitrate in seasonally upwelling waters. However, this degree of ^{15}N -
336 depletion is not recorded in subsequent sedimentary $\delta^{15}\text{N}$ values due to the integration of multiple
337 seasonal signals representing different rates of nitrate utilisation. The fact that some low $\delta^{15}\text{N}$
338 values are recorded in the Neoarchaeon sediments studied here suggests that ammonium had
339 accumulated to significant levels to remain under-utilised and that nitrogen limitation was not a
340 significant factor in the wider oceans.

341 Intriguingly, widespread partial assimilation of ammonium could have left the residual pool of NH_4^+
342 relatively ^{15}N -enriched (e.g., Yang et al., 2019). If transported offshore, uptake from a pool of heavier

343 NH_4^+ could generate ^{15}N -enriched organic matter in more distal ocean settings (Fig. 4A, B; e.g.,
344 Busigny et al., 2013). This was illustrated numerically by Yang et al. (2019) using a simple Rayleigh
345 model based on the experimental calibrations of isotope effects during ammonium uptake (Hoch et
346 al., 1992). This scenario provides an alternative explanation for the presence of positive $\delta^{15}\text{N}$ values
347 recorded in relatively distal Neoproterozoic settings in the Griqualand West Basin (e.g., Godfrey and
348 Falkowski, 2009).

349 The majority of our $\delta^{15}\text{N}$ data point to a largely anaerobic marine N cycle, driven by N_2 fixation and
350 varying degrees of ammonium uptake and recycling. However, a handful of carbonate-rich facies
351 show positive $\delta^{15}\text{N}_{\text{org}}$ values outside the range of typical values for N_2 fixation (up to +3.2‰; Fig. 4,
352 Table S1). Elevated $\delta^{15}\text{N}$ values could indicate syn-depositional oxidative degradation (Freudenthal et
353 al., 2001; Möbius et al., 2010). However, these $\delta^{15}\text{N}_{\text{org}}$ values could hint at the potential influence of
354 nitrification and incomplete denitrification in localised, mildly-oxygenated settings during the
355 deposition of carbonates, potentially periods when waters were likely shallower than when thin
356 muds were deposited. Ergolu et al. (2017) have argued that large differences in $\delta^{13}\text{C}_{\text{org}}$ values
357 between carbonates and mudstones in the shallower parts of the Campbellrand-Malmani Platform
358 were due to different consortia of microbes that comprise microbial mats in the two settings. They
359 suggested that during the deposition of carbonates, microbial mats could have had larger
360 proportions of oxygenic photoautotroph than during the deposition of mudrocks, with anaerobic
361 microbes more prevalent during the deposition of the latter. This scenario could support shallow
362 microbial mat communities as epicentres of highly localised nitrification-denitrification, without a
363 major role for aerobic N cycling in the Late Archean.

364 **6. Conclusions**

365 Here we describe the Neoproterozoic nitrogen cycle in a shallow marginal marine setting, during the
366 evolution of a well-defined carbonate platform into a relatively isolated platform- top/ rimmed-shelf
367 lagoonal environment. Nitrogen isotope values range from -3.3 to +3.2‰ and are consistent with a

368 predominantly anaerobic nitrogen cycle, dominated by N₂ fixation and the assimilation and recycling
369 of upwelling NH₄⁺. Evidence for the presence of oxidised nitrogen species is limited, suggesting that
370 any NO₃⁻ generated during periods of transient oxygen availability was quantitatively removed by
371 anaerobic respiration. However, rare δ¹⁵N values > 0 ‰ recorded in carbonate-rich sediments hint at
372 highly localized areas of nitrification and partial denitrification. In addition, the inclusion of some
373 very light δ¹⁵N values suggest partial assimilation of an upwelling pool of ammonium, leaving a
374 residual pool of ¹⁵N-enriched NH₄⁺ that could potentially explain small increases in δ¹⁵N from
375 contemporaneous open-ocean settings. We thus conclude that N cycling in the shore-proximal
376 marine environment of the Griqualand West basin was controlled by anaerobic processes and
377 recycling of bioavailable nitrogen, and that nitrification/denitrification was unlikely to have been
378 widespread prior to the end of the Neoproterozoic.

379

380 **Acknowledgements**

381 This study was supported financially by NERC Fellowship NE/H016805/2 (to AZ), NERC Standard Grant
382 NE/J023485/2 (to AZ and MC), NSF EAR-1455258 (to CKJ).

383 We would like to thank the anonymous reviewers for their careful and detailed comments.

384

385

386 **References**

387 Ader, M., Thomazo, C., Sansjofre, P., Busigny, V., Papineau, D., Laffont, R., Cartigny, P., Halverson,
388 G.P., 2016. Interpretation of the nitrogen isotopic composition of Precambrian sedimentary rocks:
389 Assumptions and perspectives. *Chem. Geol.* 429, 93 - 110.

390

391 Altabet, M.A., 1988. Variations in nitrogen isotopic composition between sinking and suspended
392 particles: Implications for nitrogen cycling and particle transformation in the open ocean. *Deep Sea*
393 *Res. A.* 35, 535 – 554.

394

395 Altabet, M.A., Francois, R., 1994. Sedimentary nitrogen isotopic ratio as a recorder for surface ocean
396 nitrate utilization. *Global biogeochemical cycles* 8, 103 – 116.

397

398 Altermann, W., Siegfried, H.P., 1997. Sedimentology and facies development of an Archaean shelf:
399 carbonate platform transition in the Kaapvaal Craton, as deduced from a deep borehole at Kathu,
400 South Africa. *J. Afr. Earth Sci.*, 24, 391 - 410.

401

402 Armstrong, R.A., Compston, W., Retief, E.A., Williams, I.S., Welke, H.J., 1991. Zircon ion microprobe
403 studies bearing on the age and evolution of the Witwatersrand triad. *Precamb. Res.* 53, 243 - 266.

404

405 Barton, J.M.J., Blignaut, E., Salnikova, E.B., Kotov, A.B., 1995. The stratigraphical position of the
406 Buffelsfontein Group based on field relationships and chemical and geochronological data. *S. Afr. J.*
407 *of Geol.* 98, 386 - 392.

408

409 Bauersachs, T., Schouten, S., Compaoré, J., Wollenzien, U., Stal, L.J., Damsteé, J.S.S., 2009. Nitrogen
410 isotopic fractionation associated with growth on dinitrogen gas and nitrate by cyanobacteria. *Limnol.*
411 *Oceanogr.* 5, 1403 - 1411.

412

413 Brunner, B., Contreras, S., Lehmann, M.F., Matantseva, O., Rollog, M., Kalvelage, T., Klockgether, G.,
414 Lavik, G., Jetten, M.S.M., Kartal, B., Kuypers M.M., 2013. Nitrogen isotope effects induced by
415 anammox bacteria. *P.N.A.S.* 110, 18994 - 18999.

416

417 Busigny, V., Lebeau, O., Ader, M., Krapez, B., Bekker, A., 2013. Nitrogen cycle in the Late Archean
418 ferruginous ocean. *Chem. Geol.* 362, 115 - 130.

419

420 Button, A., 1973. The stratigraphic history of the Malmani dolomite in the eastern and north-eastern
421 Transvaal. *Verh. Geol. Ver. S.-Afr.* 76, 229 - 247.

422

423 Casciotti, K.L. 2009. Inverse kinetic isotope fractionation during bacterial nitrite oxidation. *Geochim.*
424 *Cosmochim. Acta.* 73, 2061 - 2076.

425

426 Cline, J.D., Kaplan I.R., 1975. Isotopic fractionation of dissolved nitrate during denitrification in the
427 eastern tropical north Pacific Ocean. *Marine Chem.* 3, 271 - 299.

428

429 Czaja, A.D., Johnson, C.M., Roden, E.E., Beard, B.L., Voegelin, A.R., Nägler, T.F., Beukes, N.J., Wille,
430 M., 2012. Evidence for free oxygen in the Neoproterozoic ocean based on coupled iron–molybdenum
431 isotope fractionation. *Geochim. Cosmochim. Acta.* 86, 118 - 137.

432

433 Eroglu, S., Schoenberg, R., Wille, M., Beukes, N., Taubald, H., 2015. Geochemical stratigraphy,
434 sedimentology, and Mo isotope systematics of the ca. 2.58–2.50 Ga-old Transvaal Supergroup
435 carbonate platform, South Africa. *Precamb. Res.* 266, 27 - 46.

436

437 Eroglu, S. van Zuilen, M.A., Taubald, H., Drost, K., Wille, M., Swanner, E.D., Beukes, N.J., Schoenberg,
438 R., 2017. Depth-dependent $\delta^{13}\text{C}$ trends in platform and slope settings of the Campbellrand-Malmani
439 carbonate platform and possible implications for Early Earth oxygenation. *Precamb. Res.* 302, 122 -
440 139.

441

442 Farquhar, J., Zerkle, A.L., Bekker, A., 2011. Geological constraints on the origin of oxygenic
443 photosynthesis. *Photosynth. Res.* 107, 11 - 36.

444

445 Fischer, W.W., Schroeder, S., Lacassie, J.P., Beukes, N.J., Goldberg, T., Strauss, H., Horstmann, U.E.,
446 Schrag, D.P., Knoll, A.H., 2009. Isotopic constraints on the Late Archean carbon cycle from the
447 Transvaal Supergroup along the western margin of the Kaapvaal Craton, South Africa. *Precambrian*
448 *Res.* 169 15 - 27.

449

450 Fischer, W.W., Knoll, A.H., 2009. An iron shuttle for deep water silica in Late Archean and early
451 Paleoproterozoic iron formation. *G.S.A. Bull.* 121, 222 - 235.

452

453 Flores, E., Frías, J.E., Rubio, L.M., Herrero, A., 2005. Photosynthetic nitrate assimilation in
454 cyanobacteria. *Photosynth. Res.* 83: 117 – 133.

455

456 Freudenthal, T., Wagner, T., Weinzhöffer, F., Zabel, M., Wefer, G., 2001. Early diagenesis of organic
457 matter from sediments of the eastern subtropical Atlantic: Evidence from stable nitrogen and carbon
458 isotopes. *Geochim. Cosmochim. Acta.* 65, 1795 - 1808.

459

460 Galbraith, E.D., Kienast, M., & The NICOPP working group members, 2013. The acceleration of
461 oceanic denitrification during deglacial warming. *Nat. Geosci.* 6, 579 - 584.

462

463 Garvin, J., Buick, R., Anbar, A.D., Arnold, G.L., Kaufman, A.J., 2002. Isotopic evidence for an aerobic
464 nitrogen cycle in the latest Archean. *Science.* 323, 1045 - 1048.

465

466 Godfrey, L.V., Falkowski, P.G., 2009. The cycling and redox state of nitrogen in the Archaean ocean.
467 *Nat. Geosci.* 2, 735 - 729.

468

469 Granger, J., Sigman, D.M., Lehmann, M.F., Tortell P.D., 2008. Nitrogen and oxygen isotope
470 fractionation during dissimilatory nitrate reduction by denitrifying bacteria. *Limnol. Oceanogr.* 53,
471 2533 - 2545.

472

473 Higgins, M.B., Robinson, R.S., Husson, J.M., Carter, S.J., Pearson, A., 2012. Dominant eukaryotic
474 export production during ocean anoxic events reflects the importance of recycled NH_4^+ . *PNAS.* 109,
475 2269 - 2274.

476

477 Hoch, M.P., Fogel, M.L., Kirchman, D.L., 1992. Isotope fractionation associated with ammonium
478 uptake by a marine bacterium. *Limnol. Oceanogr.* 37, 1447 - 1459.

479

480 Izon, G., Zerkle, A.L., Zhelezinskaia, I., Farquhar, J., Newton, R.J., Poulton, S.W., Eigenbrode, J.L.,
481 Claire, M.W., 2015. Multiple oscillations in Neoproterozoic atmospheric chemistry. *E.P.S.L.* 431, 264 -
482 273.

483

484 Kendall, B., Reinhard, C.T., Lyons, T.W., Kaufman, A.J., Poulton, S.W., Anbar, A.D., 2010. Pervasive
485 oxygenation along late Proterozoic ocean margins. *Nat. Geosci.* 3, 647-652.

486

487 Knoll, A.H., Beukes, N.J., 2009. Introduction: Initial investigations of a Neoproterozoic shelf margin-basin
488 transition (Transvaal Supergroup, South Africa). *Precamb. Res.* 169, 1 - 14.

489

490 Luo, G., Shuhei Ono, S., Nicolas J. Beukes, N.J., David T. Wang, D.T., Shucheng Xie, S., Summons, R.E.
491 2016. Rapid oxygenation of Earth's atmosphere 2.33 billion years ago. *Science Advances* 13, 2,
492 e1600134

493

494 Luo, G., Junium, C.K., Izon, G., Ono, S., Beukes, N.J., Algeo, T.J., Cui, Y., Xie, S., Summons, R.E., 2018.
495 Nitrogen fixation sustained productivity in the wake of the Palaeoproterozoic Great Oxygenation
496 Event. *Nat. Comms.* 9, 978.

497

498 McCready, R.G.L., Gould, W.D., Barendregt, R.W., 1983. Nitrogen isotope fractionation during the
499 reduction of NO_3^- to NH_4^+ by *Desulfovibrio* sp. *Canadian Jour. Microbiol.* 29, 231 - 234.

500

501 Miyano, T., Beukes, N.J., 1984. Phase relations of stilpnomelane, ferri-annite, and riebeckite in very
502 low grade metamorphosed iron formations. *Verh. Geol. Ver. S.-Afr.* 87, 111 - 124.

503

504 Möbius, J., Lahajnar, N., Emeis K-C., 2010. Diagenetic control of nitrogen isotope ratios in Holocene
505 sapropels and recent sediments from the Eastern Mediterranean Sea. *Biogeosci.* 7, 3901 - 3914.

506

507 Möbius, J., 2013. Isotope fractionation during nitrogen remineralization (ammonification):
508 implications for nitrogen isotope biogeochemistry. *Geochim. Cosmochim. Acta.* 105, 422-432.

509

510 Pavlov, A.A., Kasting, J.F., 2002. Mass-independent fractionation of sulfur isotopes in Archean
511 sediments: strong evidence for an anoxic Archean atmosphere. *Astrobiology.* 2, 27 - 41.

512

513 Peters, K.E., Sweeney, R.E., Kaplan, I.R., 1978. Correlation of carbon and nitrogen stable isotope
514 ratios in sedimentary organic matter. *Limn. Ocean.* 23, 598 - 604.

515

516 Polissar, P.J., Fulton, J.M., Junium, C.K., Courtney C. Turich, C.C., Freeman, K.H., 2009. Measurement
517 of ^{13}C and ^{15}N Isotopic Composition on Nanomolar Quantities of C and N. *Anal. Chem.* 81, 755 - 763.

518

519 Rau, G.H., Sullivan, W., Gordon, L.I., 1991. $\delta^{13}\text{C}$ and $\delta^{15}\text{N}$ variations in Weddell Sea particulate
520 organic matter. *Marine Chemistry*, 35, 355 – 369.

521

522 Sigman, D. M., Robinson, R., Knapp, A.N., van Geen, A., McCorkle, D. C., Brandes, J.A., Thunell, R.C.,
523 2003. Distinguishing between water column and sedimentary denitrification in the Santa Barbara
524 Basin using the stable isotopes of nitrate. *Geochem. Geophys. Geosys.* 4, 1040.

525

526 Sigman, D.M., Karsh, K.L., Casciotti, K.L., 2009. Ocean process tracers: Nitrogen isotopes in the
527 ocean. In: Steele, J.H., Turekian, K.K., (Eds.) *Encyclopedia of Ocean Sciences*. London: Academic
528 Press.

529

530 Stüeken, E.E., Kipp, M.A., Koehler, M.C., Buick, R., 2016. The evolution of Earth's biogeochemical
531 nitrogen cycle. *Earth Sci. Rev.*, 160, 220 - 239.

532

533 Stüeken, E.E., Zalomis, J., Meixnerová, J., Buick, R., 2017. Differential metamorphic effects on
534 nitrogen isotopes in kerogen extracts and bulk rocks. *Geochim. Cosmochim. Acta.* 217, 80 - 94.

535

536 Sumner, D.Y., Grotzinger, J.P., 2004. Implications for Neoproterozoic ocean chemistry from primary
537 carbonate mineralogy of the Campbellrand-Malmani Platform, South Africa. *Sedimentology.* 51,
538 1273 - 1299.

539

540 Sumner, D.Y., Beukes, N.J., 2006. Sequence stratigraphic development of the Neoproterozoic Transvaal
541 carbonate platform, Kapvaal Craton, South Africa. *S. Afr. J. Geol.* 109, 11 - 22.

542

543 Thomazo, C., Ader, M., Philippot, P., 2011. Extreme ¹⁵N-enrichments in 2.72-Gyr-old sediments:
544 evidence for a turning point in the nitrogen cycle. *Geobiology*. 9, 107 - 120.

545

546 Walraven, F. and Martini, J., 1995. Zircon Pb-evaporation age determinations of the
547 Oak Tree Formation, Chuniesport Group, Transvaal Sequence: Implications for Transvaal-Griqualand
548 West basin correlations. *S. Afr. J. of Geol.* 98, 58 - 67.

549

550 Walter M., Grotzinger J.P., Schopf J.W., 1992. Proterozoic stromatolites. In: Schopf J.W., Klein C.
551 (Eds.), *The Proterozoic biosphere. A multidisciplinary study*, Cambridge Univ. Press, Cambridge. 253 -
552 260.

553

554 Weber, T., Deutsch, C., 2014. Local versus basin-scale limitation of marine nitrogen fixation. *P.N.A.S.*
555 111, 8741 - 8746.

556

557 Yang, J., C. K. Junium, C.K., Grassineau, N.V., Nisbet, E.G., Izon, G., Mettam, C., Martin, A., Zerkle,
558 A.L., 2019. Ammonium availability in the Late Archaean nitrogen cycle. *Nat. Geosci.*
559 <https://doi.org/10.1038/s41561-019-0371-1>

560

561 Zerkle, A.L., Junium, C.K., Canfield, D.E., House, C.H., 2008. Production of ¹⁵N-depleted biomass
562 during cyanobacterial N₂-fixation at high Fe concentrations. *Jour. Geophys. Res.* 113,
563 doi:10.1029/2007JG000651.

564

565 Zerkle, A.L., Claire, M.W., Domagal-Goldman, S.D., Farquhar, J., Poulton, S. W., 2012. A bistable
566 organic-rich atmosphere on the Neoproterozoic Earth. *Nat. Geosci.* 5, 359 - 363.

567

568 Zerkle, A.L., Poulton, S.W., Newton, R.J., Mettam, C., Claire, M.W., Bekker, A., Junium, C.K., 2017.
569 Onset of the aerobic nitrogen cycle during the Great Oxidation Event. *Nature.* 542, 465 - 467.

570

571 Zhang, X., Sigman, D.M., Morel, F.M., Kraepiel, A.M., 2014. Nitrogen isotope fractionation by
572 alternative nitrogenases and past ocean anoxia. *P.N.A.S.* 111, 4782 - 4787.

573

574

575

576

577

578

579

580

581

582 Figure Legends

583 **Fig 1.** (A) Simplified stratigraphy of BH1-Sacha core (Altermann and Siegfried, 1997). (B) Simplified
584 structure of Campbellrand-Malmani platform-top and ramp showing placement of BH1-Sacha core
585 (Sumner and Beukes, 2006). (C) Position of BH1-Sacha drill site (star symbol) in South Africa (Sumner
586 and Beukes, 2006). Dates in Figs. A and B are from a review in Sumner and Beukes (2009). More
587 dates and references from correlative stratigraphy are presented in the supplementary information
588 which confirm a date of 2588 to 2549 Ma for the Monteville Fm.

589

590 **Fig. 2.** Geochemical data for BH1-Sacha core. Nitrogen isotope data $\delta^{15}\text{N}_{\text{org}}$ (‰) are shown as black
591 dots for silicates and triangles for carbonates, whilst $\delta^{15}\text{N}_{\text{bulk}}$ (‰) are shown as open pentagons).
592 Carbonate abundance data (wt. %) are shown as dots. TOC (wt. %) and $\delta^{13}\text{C}_{\text{org}}$ (‰) data from this
593 study are shown as dots, whilst data from Izon et al. (2015) are shown as open squares. Symbols for
594 lithologies in core diagram as per Fig. 1A. Error bars for $\delta^{15}\text{N}_{\text{org}}$ reflect the combined standard
595 deviation of N1 standards and triplicates of sample BH1-1963.6 using the equation: error bar = $\sqrt{}$

596 **Fig. 3.** Cross plots of geochemical data. Filled circles represent data from this study. Open squares
597 include TOC and $\delta^{13}\text{C}_{\text{org}}$ data from Izon et al. (2015). Data shown: (A) TN_{org} and $\delta^{15}\text{N}_{\text{org}}$, (B) $\delta^{15}\text{N}_{\text{org}}$
598 and $\delta^{13}\text{C}_{\text{org}}$, (C) $\text{TOC}/\text{TN}_{\text{org}}$ and $\delta^{15}\text{N}_{\text{org}}$ (D) TOC and $\delta^{13}\text{C}_{\text{org}}$, (E) TN_{bulk} and $\delta^{15}\text{N}_{\text{bulk}}$, (F) $\delta^{15}\text{N}_{\text{bulk}}$ and
599 $\delta^{13}\text{C}_{\text{org}}$, (G) potassium and $\delta^{15}\text{N}_{\text{bulk}}$ and (H) TN_{bulk} and $\delta^{15}\text{N}_{\text{bulk}}$.

600

601 **Fig. 4.** Proposed model for facies-dependent nitrogen cycling at the ocean margin. This depositional
602 setting is a well-defined marine marginal ramp and platform-top that could have reduced
603 communication with the open ocean and led to somewhat isolated shallow **depositional settings**.
604 Platform/ramp bathymetry and stromatolite assemblages are based upon idealised Proterozoic
605 ramp and platform settings by Walter et al. (1992). Shown here are: **(A)** a shallow ramp top setting,
606 representing the Schmidtsdrift Subgroup and Monteville Fm; and **(B)** a lagoonal depositional setting,
607 representing the Campbellrand Subgroup overlying the Monteville Fm. The proposed mechanisms
608 include: **(1)** transport of diazotrophic biomass to the seafloor; **(2)** remineralization of OM to NH_4^+
609 and shoreward transport; **(3)** NH_4^+ assimilation, producing OM with -ve $\delta^{15}\text{N}$ values; **(4)** transport of
610 a residual pool of NH_4^+ (possibly with +ve $\delta^{15}\text{N}$ values); **(5)** open ocean ammonium assimilation,
611 producing OM with +ve $\delta^{15}\text{N}$ values; and, **(6)** potential for restricted open-marine influence but **(7)**
612 potential for variability in communication as sea levels fluctuated.

613

614

615

616

617

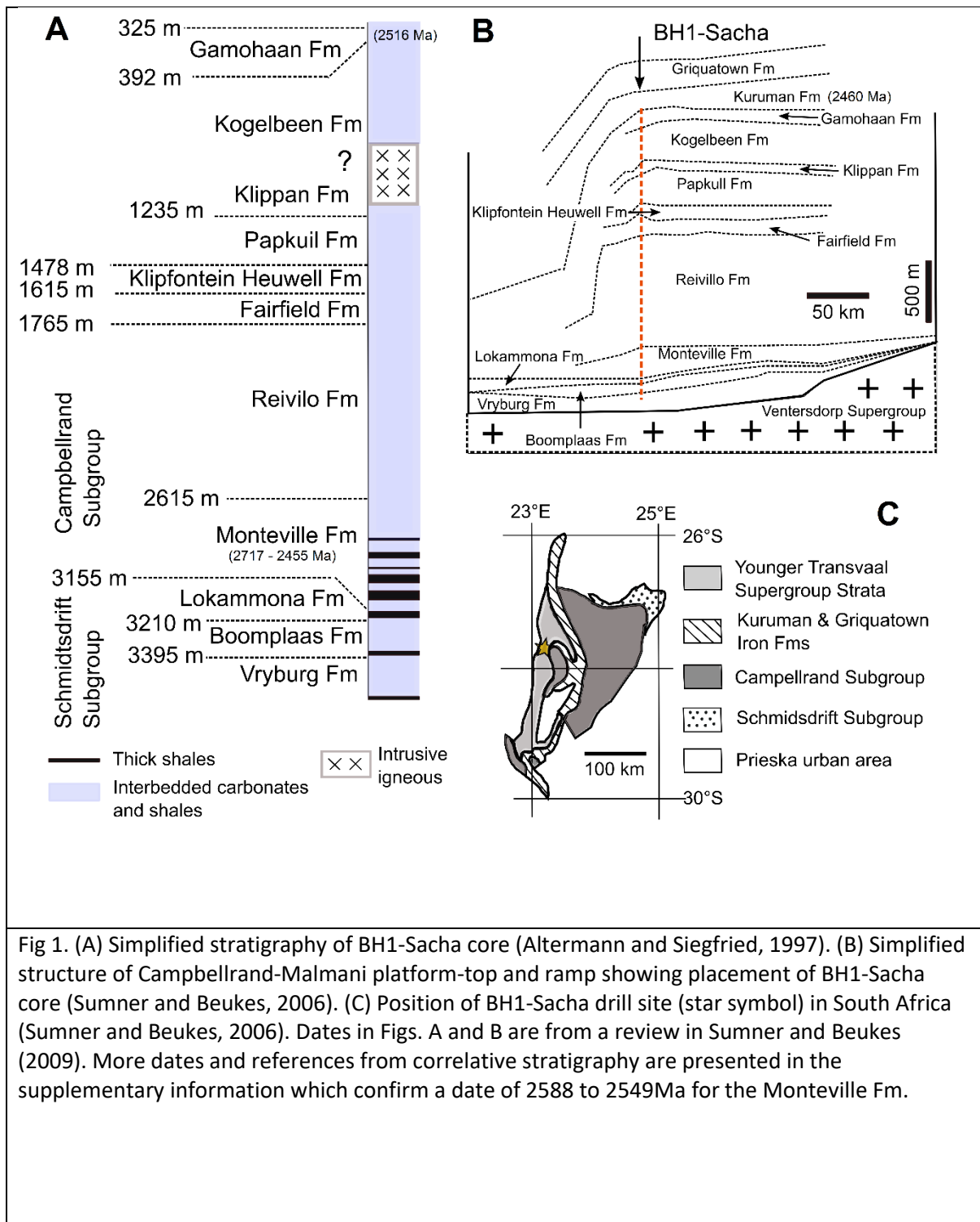


Fig 1. (A) Simplified stratigraphy of BH1-Sacha core (Altermann and Siegfried, 1997). (B) Simplified structure of Campbellrand-Malmani platform-top and ramp showing placement of BH1-Sacha core (Sumner and Beukes, 2006). (C) Position of BH1-Sacha drill site (star symbol) in South Africa (Sumner and Beukes, 2006). Dates in Figs. A and B are from a review in Sumner and Beukes (2009). More dates and references from correlative stratigraphy are presented in the supplementary information which confirm a date of 2588 to 2549Ma for the Monteville Fm.

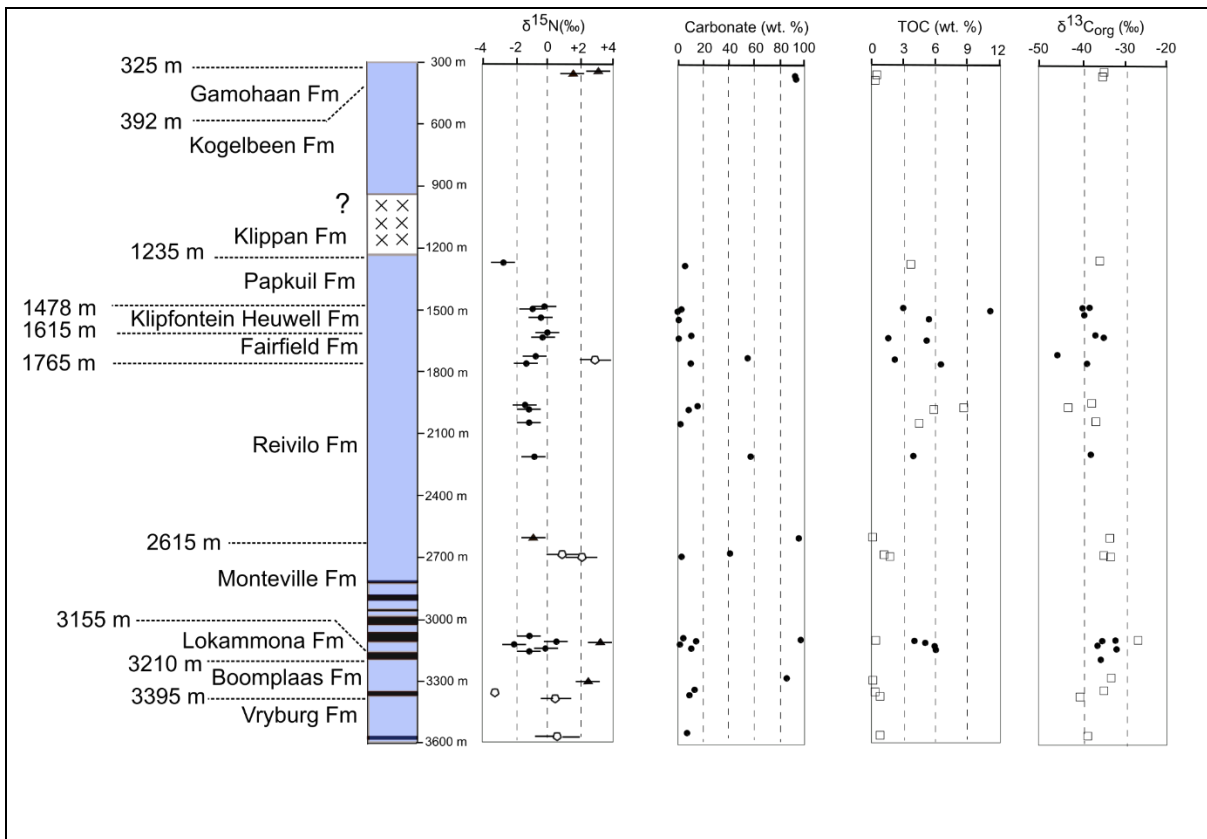


Fig. 2. Geochemical data for BH1-Sacha core. Nitrogen isotope data $\delta^{15}\text{N}_{\text{org}}$ (‰) are shown as black dots for silicates and triangles for carbonates, whilst $\delta^{15}\text{N}_{\text{bulk}}$ (‰) are shown as open pentagons). Carbonate abundance data (wt. %) are shown as dots. TOC (wt. %) and $\delta^{13}\text{C}_{\text{org}}$ (‰) data from this study are shown as dots, whilst data from Izon et al. (2015) are shown as open squares. Symbols for lithologies in core diagram as per Fig. 1A. Error bars for $\delta^{15}\text{N}_{\text{org}}$ reflect the combined standard deviation of N1 standards and triplicates of sample BH1-1963.6 using the equation: error bar = $\sqrt{(\text{error of standards}^2 + \text{largest error of corrected sample}^2)}$. Error bars are thus $\pm 0.7\text{‰}$. Error bars for $\delta^{15}\text{N}_{\text{bulk}}$ reflect the combined standard deviation of standards and the intercept errors of keeling plots for each sample triplicate using the same formula. These are shown in the supplementary tables.

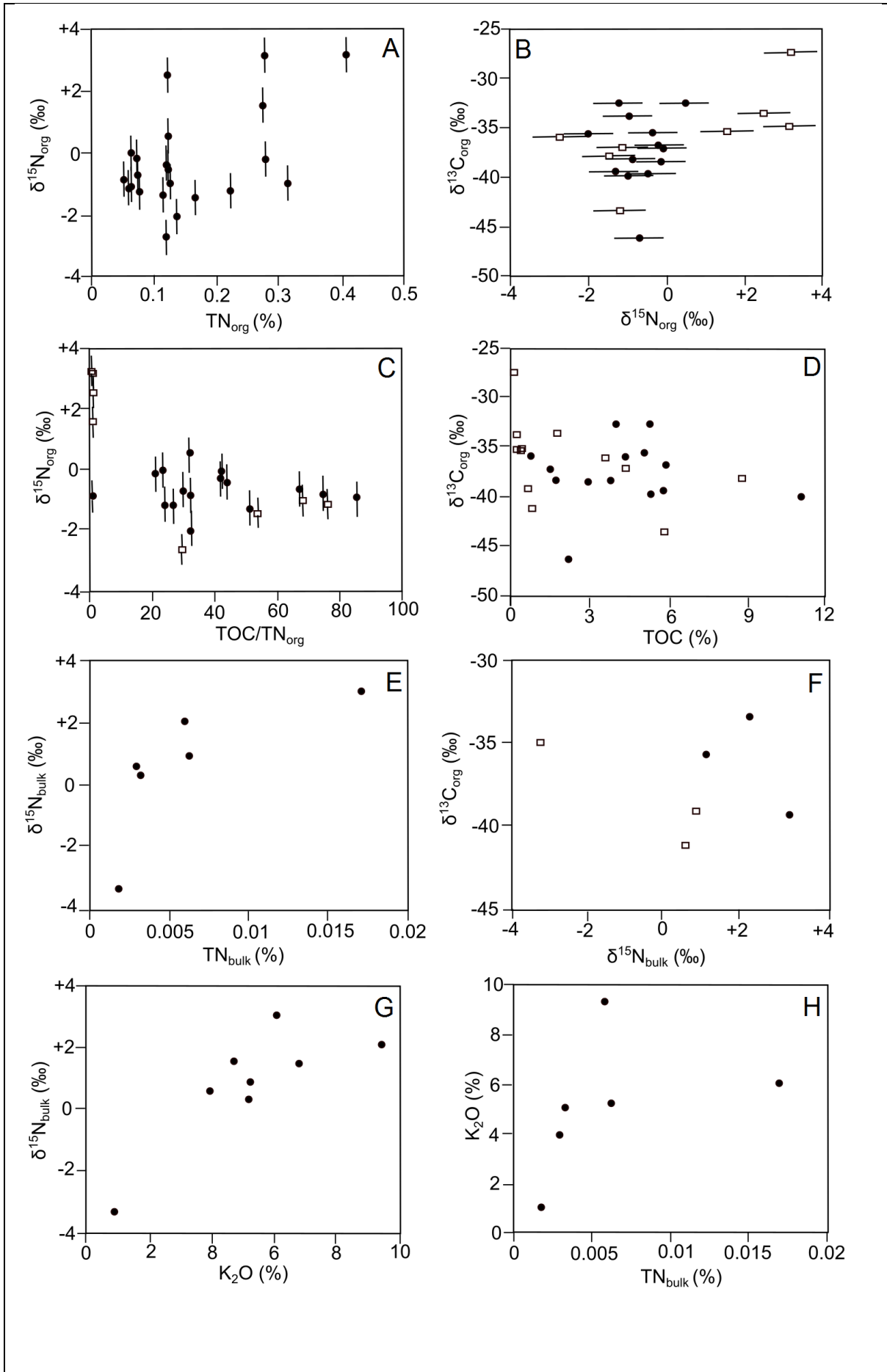


Fig. 3. Cross plots of geochemical data. Filled circles represent data from this study. Open squares include TOC and $\delta^{13}\text{C}_{\text{org}}$ data from Izon et al. (2015). Data shown: (A) TN_{org} and $\delta^{15}\text{N}_{\text{org}}$, (B) $\delta^{15}\text{N}_{\text{org}}$ and $\delta^{13}\text{C}_{\text{org}}$, (C) $\text{TOC}/\text{TN}_{\text{org}}$ and $\delta^{15}\text{N}_{\text{org}}$ (D) TOC and $\delta^{13}\text{C}_{\text{org}}$, (E) TN_{bulk} and $\delta^{15}\text{N}_{\text{bulk}}$, (F) $\delta^{15}\text{N}_{\text{bulk}}$ and $\delta^{13}\text{C}_{\text{org}}$, (G) potassium and $\delta^{15}\text{N}_{\text{bulk}}$ and (H) TN_{bulk} and $\delta^{15}\text{N}_{\text{bulk}}$.

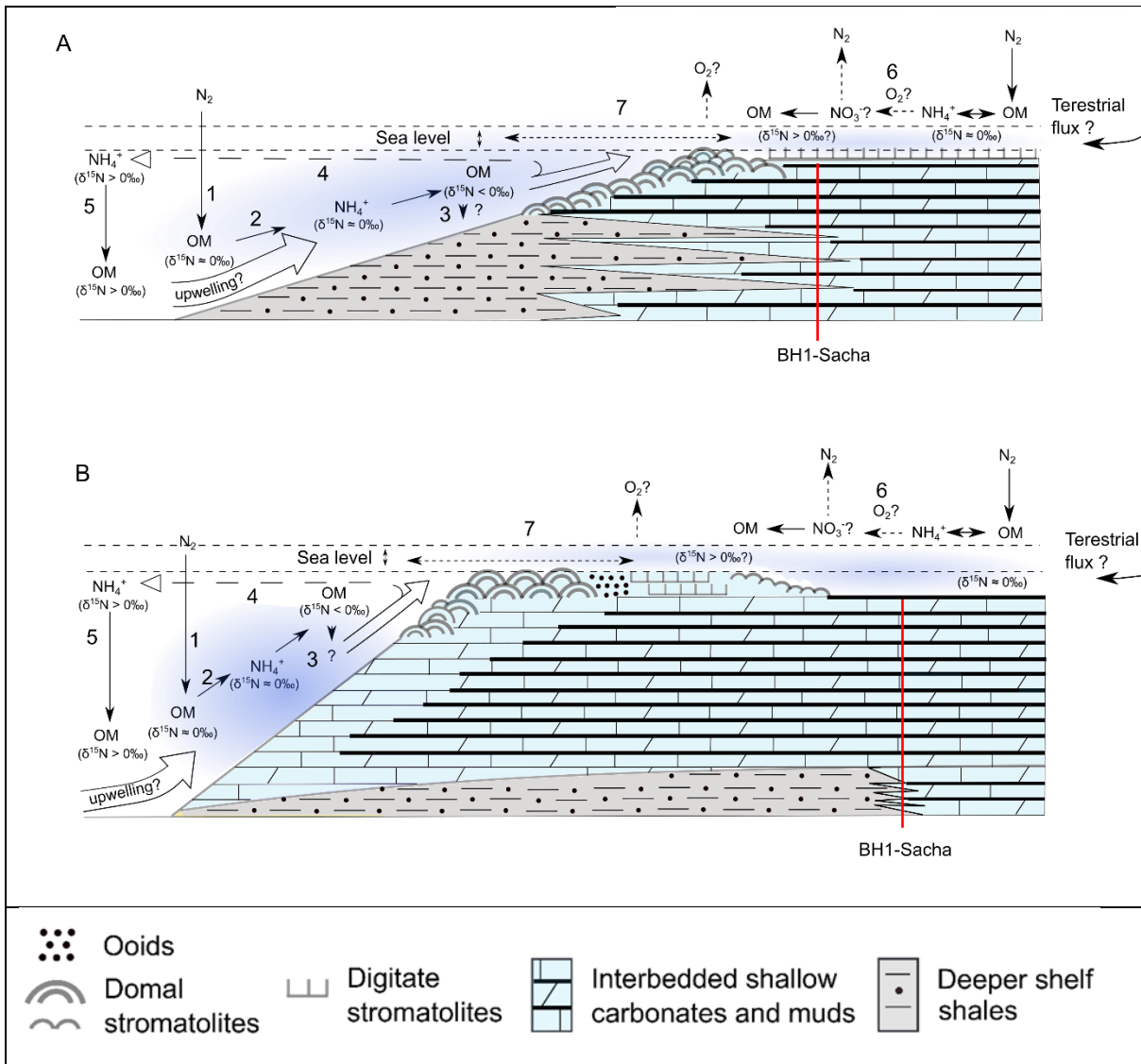


Fig. 4. Proposed model for facies-dependent nitrogen cycling at the ocean margin. This depositional setting is a well-defined marine marginal ramp and platform-top that could have reduced communication with the open ocean and led to somewhat isolated shallow depositional settings. Platform/ramp bathymetry and stromatolite assemblages are based upon idealised Proterozoic ramp and platform settings by Walter et al. (1992). Shown here are: **(A)** a shallow ramp top setting, representing the Schmidrift Subgroup and Monteville Fm; and **(B)** a lagoonal depositional setting, representing the Campbellrand Subgroup overlying the Monteville Fm. The proposed mechanisms include: **(1)** transport of diazotrophic biomass to the seafloor; **(2)** remineralization of OM to NH_4^+ and shoreward transport; **(3)** NH_4^+ assimilation, producing OM with -ve $\delta^{15}\text{N}$ values; **(4)** transport of a residual pool of NH_4^+ (possibly with +ve $\delta^{15}\text{N}$ values); **(5)** open ocean ammonium assimilation, producing OM with +ve $\delta^{15}\text{N}$ values; and, **(6)** potential for

restricted open-marine influence but **(7)** potential for variability in communication as sea levels fluctuated.

624

625

626